Sequential Assignment and Structure Determination of Spider Toxin ω-Aga-IVB[†,‡]

Hongtao Yu,[§] Michael K. Rosen,[§] Nicholas A. Saccomano,[∥] Douglas Phillips,[∥] Robert A. Volkmann,[∥] and Stuart L. Schreiber*[,§]

Department of Chemistry, Harvard University, 12 Oxford Street, Cambridge, Massachusetts 02138, and Departments of Medicinal Chemistry and Neuroscience, Pfizer Central Research, Groton, Connecticut 06340

Received July 29, 1993; Revised Manuscript Received September 13, 1993[⊗]

ABSTRACT: The solution structure of a peptide toxin isolated from funnel web spider venom, ω-Aga-IVB, was determined by 2D NMR methods. ω-Aga-IVB is a high-affinity specific blocker of P-type voltage-dependent calcium channels. Nearly all of the proton resonances of this 48-residue protein were assigned using conventional 2D homonuclear NMR experiments. The three-dimensional structure of the molecule was determined by simulated annealing. The distance and dihedral restraints used in the structure calculations were derived from NOESY and COSY-type experiments, respectively. Mass spectrometric analysis of ω-Aga-IVB suggests that the protein contains four disulfide bonds. In the absence of chemical data to identify the pattern of cysteine pairing, the disulfide bonds of the toxin are proposed from the NMR data and subsequent structural calculations. The structure of the toxin can be described as a three-stranded anti-parallel β sheet connected by flexible loops. A striking feature of the structure is that the C-terminal 10 residues of this protein adopt random coil conformations. Several positively charged amino acid side chains are found localized on one face of the molecule, in close proximity to the C-terminal tail. This observation has led us to propose a speculative model of the toxins blockade mechanism.

Calcium ion entry into excitable cells is largely regulated by voltage-gated ion channel proteins located in the plasmalemma (Bean, 1989; Hess, 1990). Multiple subtypes of calcium channels colocalize on excitable cells (Tsien et al., 1988; Miller, 1992) and are required for producing several diverse cellular and physiological responses including membrane excitability (Llinas, 1988), enzyme activation (Kennedy, 1989), neurotransmitter and hormone release (Augustine et al., 1987; Turner et al., 1992), muscle contraction (Catterall, 1991a), gene expression (Murphy et al., 1991), neurite outgrowth (Kater et al., 1988), and cell death (Weiss et al., 1990). Current identification and functional characterization of Ca^{2+} channel subtypes use electrophysiological, molecular, and pharmacological criteria (Tsien et al., 1991; Dubel et al., 1992; Williams et al., 1992; Barry et al., 1993). Based on these discriptors, three classes of neuronal high voltage-activated calcium channels have been proposed (P-, L-, and N-).

The use of venom toxins as essential tools for identification and understanding of cation channels is well documented (Catterall, 1984; Castle et al., 1989; Spedding & Paoletti, 1992). The cone-snail toxin, ω-CgTx-GVIA[1] (Olivera et al., 1984) and the recently reported spider toxin ω-Aga-IVA (Mintz et al., 1992; Burke et al., 1992) have provided the pharmacological means for identification and blockade of N- and P-type calcium channels, respectively. Currents recorded from the Purkinje cell of the cerebellum are resistant to the N-channel antagonist ω-CgTx-GVIA and the DHP L-channel antagoninsts (e.g., nifedipine) but are sensitive to ω-Aga-IVA (Llinas et al., 1989; Regan et al., 1991b). Recent studies suggest that the P-channel [termed as such to reflect the cell (Purkinje) of origin (Llinas et al., 1992) and characterized by sensitivity to ω-Aga-IVA and resitance to ω-CgTx-GIVA and DHP blockade] is more broadly distributed in the nervous system (Regan, 1991a) and is functionally coupled to neurotransmitter release and synaptic tramsmission (Turner et al., 1992; Burke et al., 1992; Hirning et al., 1992).

Agelenopsis aperta venom contains a family of 48 amino acid toxins related to ω-Aga-IVA. The most abundant member is designated Agel K which shares greater than 70% amino acid identity with ω-Aga-IVA and maintains a similar pharmacological profile (Phillips et al., 1992; Hirning et al., unpublished results; Ganong et al., unpublished results). To acknowledge the prior literature (Mintz et al., 1992), we will henceforth term Agel K, ω-Aga-IVB. The emerging importance of P-channels in central function and the unique utility of this class of toxins for the study of P-channel structure and function has generated an immense interest in these toxin molecules. Herein we report the sequential assignment and solution structure of ω-Aga-IVB.

The primary sequence of ω-Aga-IVB is shown in Figure 2. Although mass spectroscopic data indicate the presence of four disulfide bonds (Hirning et al., unpublished results), it has not been possible to obtain the disulfide pairing information using classical enzymatic or chemical techniques due to the high density of cysteines in the protein. The most reasonable pattern of the disulfide bonds based on our NMR data is Cys4–Cys20, Cys12–Cys25, Cys19–Cys36, and Cys27–Cys34. The molecule contains a small three-stranded antiparallel β sheet with a topology of +2x and −1. Both the three N-terminal residues (Glu1–Asn3) and the 10 C-terminal residues (Arg39–Ala48) adopt random-coil conformations in solution. Many

[†] Supported by a grant from the National Institute of Health (GM 44993) to S.L.S.

* To whom correspondence should be addressed.

[‡] Coordinates have been deposited in the Protein Data Bank with the entry name 10MB.

[§] Harvard University.

[∥] Pfizer Central Research.

[⊗] Abstract published in *Advance ACS Abstracts*, November 1, 1993.

[1] Abbreviations: NMR, nuclear magnetic resonance; 2D, two-dimensional; COSY, homonuclear correlation spectroscopy; DQF, double-quantum filtered; DQ, double-quantum spectroscopy; NOE, nuclear Overhauser effect; NOESY, NOE spectroscopy; ppm, parts per million; TOCSY, total correlation spectroscopy; TPPI, time-proportional phase incrementation; DHP, dihydropyridine; ω-CgTx-GVIA, ω-Conotoxin GVIA; RP, reversed-phase; HPLC, high-performance liquid chromatography; UV, ultraviolet; RMSD, root mean squared deviation.

0006-2960/93/0432-13123$04.00/0

of the C-terminal residues, such as Leu40, Ile41, Met42, Leu45, and Phe47, are hydrophobic in nature. The flexible hydrophobic tail and the positively charged amino acid side chains localized on the same face of the protein suggest possible models for the channel-blocking actions of the toxin.

MATERIAL AND METHODS

Preparation of the Sample. Both male and female *A. Aperta* (Aranae, Agelenidae), a common western U.S. funnel-web spider, were milked periodically. This resulted in approximately 0.5 μL of venom per milking. Homogeneous and biologically active ω-Aga IVB was obtained from the whole venom by a three-step purification procedure using sequential gel filtration, strong cation exchange chromatography, and RP-HPLC desalting. Approximately 4 mg of protein was dissolved in 400 μL of 50 mM phosphate buffer (pH 5.0), and the pH was adjusted to 4.0 using d_4-acetic acid. The final protein concentration was approximately 2 mM as determined by UV absorbance at 280 nm. A D_2O sample was prepared by lyophilizing the H_2O sample and dissolving it in 400 μL of 99% D_2O.

NMR Spectroscopy. All NMR data were recorded at 300 K on either a Bruker AMX600 or AM500 instrument. Two-dimensional DQF-COSY (Piantini et al., 1982), DQ (τ = 32 ms) (Bax et al., 1981), relay-COSY (τ = 32 ms) (Eich et al., 1982), TOCSY (τ = 80 ms) (Bax & Davis, 1985), and NOESY (τ = 75 and 250 ms) (Jeener et al., 1979; Macura et al., 1981) spectra were acquired using standard pulse sequences. Quadrature detection in the t_1 dimension was achieved with the States-TPPI method. In all experiments, 512 t_1 increments were recorded. The NMR data were processed with the FELIX software with appropriate apodization, base line correction and zero-filling to yield real 1K × 1K matrices after reduction (Hare, 1991).

The $^3J_{NH-H\alpha}$ coupling constants were measured using a DQF-COSY spectrum recorded in H_2O. A 4K × 4K matrix was constructed by zero-filling the fingerprint region of the spectrum in both dimensions to enhance digital resolution. Proton–deuterium exchange of amide protons was studied on a sample of ω-Aga-IVB lyophilized from H_2O buffer and dissolved in pure D_2O. Immediately following the dissolution of ω-Aga-IVB into D_2O, an 80-ms TOCSY was taken which lasted 10 h. The amide protons that were visible in the processed TOCSY experiment were regarded as slowly exchanging.

Derivation of the NMR Constraints. Three-dimensional structures were calculated from the experimental restraints with the program X-PLOR 2.1, using the reported protocol (Brünger, 1990). The generated structures were refined with the simulated annealing refinement protocol described in the X-PLOR 3.1 manual (Bünger, 1993). NOE-based interproton distance restraints were derived from a 2D NOESY spectrum with a mixing time of 250 ms. The cross-peak intensities measured in a 75-ms NOESY spectrum were used to calibrate distance restraints based on known distances in regular secondary structural elements. Restraints were divided into three categories: weak (1.8 Å ≤ d ≤ 5.0 Å), medium (1.8 Å ≤ d ≤ 3.3 Å for NOEs involving aliphatic protons; 1.8 Å ≤ d ≤ 3.5 Å for NOEs involving amide protons), and strong (1.8 Å ≤ d ≤ 2.7 Å); an additional 0.5 Å was added to the upper limit for distances involving methyl protons. We used 17 side chain χ_1 and 10 backbone ϕ angle restraints; these are based on coupling constants and cross-peak magnitudes measured in a DQF-COSY spectrum, and on intraresidue NOE data (Wagner et al., 1987). In all cases, χ_1 values were restricted to a ±60° range, allowing stereospecific assignment of side chain protons based on NOEs to amide NHs and C_αHs. Three hydrogen bonds derived from the three slowly exchanging amide protons were incorporated as six distance restraints with 2.4 Å ≤ d_{N-O} ≤ 3.3 Å and 1.5 Å ≤ d_{H-O} ≤ 2.3 Å. Disulfide bonds, when included in the calculations, were represented as distance restraints with 1.92 Å ≤ d_{S-S} ≤ 2.12 Å. The set of structural restraints was built up in an iterative manner using initial structures generated with only a subset of the total restraints to resolve ambiguities in the NOE assignments.

RESULTS

Spin System Identification and Sequential Assignment. The sequential assignment was performed in two stages involving spin system identification and through-space sequential connection of the spin systems (Wüthrich, 1986; Chazin et al., 1988a,b). The magnetization transfer in the 80-ms TOCSY experiment was sufficient to provide most of the expected cross-peaks between amide NHs and their corresponding side chain protons. The excellent separation of the amide NH chemical shifts made it possible to unambiguously identify most of the spin systems on the basis of their amide NH chemical shifts. The spin systems were then tentatively assigned to amino acid types on the basis of scalar coupling patterns observed in DQF-COSY, TOCSY, and DQ experiments. The DQ spectrum was also particularly useful in identifying spin systems whose C_αHs were near the water resonance. The alanine and threonine assignments were confirmed through the observation of strong cross-peaks between methyl protons and $C_\alpha H/C_\beta H$, respectively, in the DQF-COSY spectrum. Threonines were distinguished from the alanines by the existence of the strong $C_\gamma H_3/C_\alpha H$ cross-peaks in the relay-COSY spectrum. The glycines showed remote cross-peaks at ω_2 = NH and $\omega_1 = C_{\alpha 1}H + C_{\alpha 2}H$ in a DQ spectrum recorded in H_2O. By analysis of the patterns of the strong methyl coupling peaks in the DQF-COSY, DQ, and relay-COSY spectra, the methyl resonances belonging to isoleucine and leucine residues were tentatively assigned and were correlated to their amide proton chemical shifts in the TOCSY experiments. The assignments of the aromatic resonances (Trp, Tyr, and Phe) were straightforward since each of them occurs only once in ω-Aga-IVB. The ring δ protons of the aromatic residues Tyr9 and Trp14 showed NOESY cross-peaks to their respective C_βHs, hence allowing us to correlate their ring spin systems with their main-chain spin systems. The side chain NH of arginine showed the same cross-peaks as the backbone NH in the TOCSY experiments. Tentative assignments of the serine residues were also made on the basis of their slightly lower field C_βH chemical shifts. The remaining spin systems, including the prolines, were only identified at the sequential assignment stage.

The sequential assignment of this protein was achieved through analysis of the $C_\alpha H_i$–NH_{i+1}, NH_i–NH_{i+1}, and $C_\beta H_i$–NH_{i+1} NOE connectivities. Long stretches of peptide segments could easily be traced using the 250-ms NOESY spectrum starting from unique residues. Figure 1 shows the NOE connectivities from Gly15 to Cys4. Figure 2 shows all the connections used to accomplish the sequential assignment. The sequential assignment was greatly facilitated by the completeness of the spin system identification. The sequential assignment in the β sheet region was also confirmed by the interstrand long-range NOE connectivities. The ^1H chemical shifts of ω-Aga-IVB are shown in Table I.

Secondary Structure Analysis. The regular secondary structure of ω-Aga-IVB is best described as a three-stranded

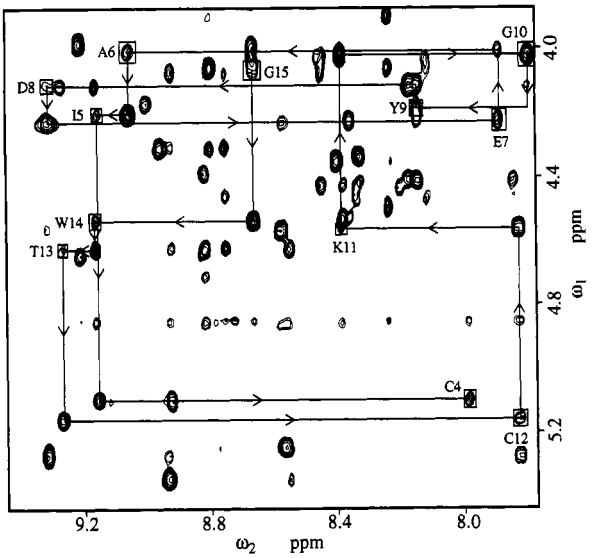

FIGURE 1: Fingerprint region of the 250-ms ^1H NOESY spectrum of ω-Aga-IVB recorded in H_2O buffer. Sequential $C_\alpha H_i$–NH_{i+1} connectivity data are shown for Cys4–Gly15. Intraresidue $C_\alpha H_i$–NH_i cross-peaks are boxed. Arrows indicate the direction of the sequential connectivity from C-terminus to N-terminus.

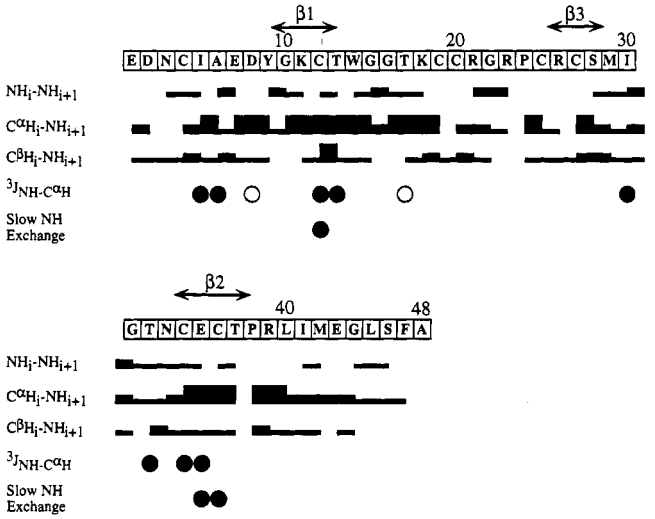

FIGURE 2: Summary of sequential NOEs, $^3J_{NH-C\alpha H}$ coupling constants, and slowly exchanging amide protons. The widths of the bars indicate the intensities of the corresponding NOEs (strong, medium, or weak). Small $^3J_{NH-C\alpha H}$ coupling constants are shown as open circles, while large $^3J_{NH-C\alpha H}$ coupling constants are shown as closed circles. Slowly exchanging amide protons are also represented by closed circles. The proposed secondary structural elements are shown above the amino acid sequence; S stands for β strand. When the calculated three-dimensional structures are analyzed for secondary structural elements with the program QUANTA, residues Lys11, Cys12, Arg26, Cys27, Cys34, Glu35, and Cys36 satisfy the hydrogen-bonding pattern and main chain torsion of extended β conformations (Kabsch & Sander, 1983).

antiparallel β sheet. The β strands were characterized by the strong sequential $C_\alpha H_i$–NH_{i+1} NOEs, the large $^3J_{NH-H\alpha}$ coupling constants, and the interstrand long-range NOE patterns ($C_\alpha H_i$–NH_j, NH_i–NH_j, and $C_\alpha H_i$–$C_\alpha H_j$). Additional support was provided by the secondary shifts of the amide NH and $C_\alpha H$ protons and the slowly exchanging amide protons (Williams, 1989; Wishart et al., 1992).

As shown in Figure 3, the three strands of the β sheet have a $+2x$, -1 topology. The long loop (from Thr13 to Pro24) connecting strand 1 and strand 2 does not seem to adopt any regular secondary structure. Long-range NOEs demonstrate that there is an association between this loop and the

Table I: ^1H Chemical Shifts[a] of Spider Toxin ω-Aga-IVB

residue	NH	$C^\alpha H$	$C^\beta H$ pro-S[b]	$C^\beta H$ pro-R	other
Glu1		4.17	2.25		$C^\gamma H$ 2.61
Asp2	9.00	4.87	2.97, 2.85		
Asn3	8.73	4.78	2.93, 2.86		$N^{\delta 2}H$ 7.69, 6.97
Cys4	7.99	5.10	*2.96	3.08	
Ile5	9.16	4.20	2.15		$C^{\gamma 2}H$ 1.05; $C^{\gamma 1}H$ 1.52, 1.23; $C^\delta H$ 0.96
Ala6	9.06	4.00	1.56		
Glu7	7.89	4.23	2.09, 1.97		$C^\gamma H$ 2.62, 2.57
Asp8	9.30	4.12	2.84, 2.52		
Tyr9	8.15	4.19	3.36, 3.18		$C^\delta H$ 7.12; $C^\epsilon H$ 6.96
Gly10	7.80	4.02, 3.36			
Lys11	8.39	4.56	1.90, 1.89		$C^\gamma H$ 1.58, 1.54; $C^\delta H$ 1.84, 1.75; $C^\epsilon H$ 3.14
Cys12	7.83	5.16	*3.46	3.42	
Thr13	9.27	4.62	4.12		$C^\gamma H$ 1.25
Trp14	9.17	4.54	3.36, 3.33		$C^{\delta 1}H$ 7.24; $N^{\epsilon 1}H$ 10.10; $C^{\epsilon 3}H$ 7.68; $C^{\eta 2}H$ 7.35; $C^{\zeta 2}H$ 7.35
Gly15	8.67	4.07, 3.73			
Gly16	7.76	4.50, 3.73			
Thr17	8.24	4.07	3.90		$C^\gamma H$ 1.38
Lys18	8.80	4.31	*1.93	2.04	$C^\gamma H$ 1.65, 1.56; $C^\delta H$ 1.80; $C^\epsilon H$ 3.11
Cys19	8.96	4.86	*2.97	3.59	
Cys20	8.83	4.64	*2.67	3.48	
Arg21	9.21	3.98	2.14, 1.86		$C^\gamma H$ 1.62, 1.62; $C^\delta H$ 3.24; $N^\epsilon H$ 7.39
Gly22	8.67	4.02, 3.84			
Arg23	7.25	4.35	1.54		$C^\gamma H$ 1.99, 1.79; $C^\delta H$ 2.78; $N^\epsilon H$ 7.58
Pro24		4.57	2.29, 1.85		$C^\gamma H$ 2.25, 2.11; $C^\delta H$ 4.28, 3.75
Cys25	8.58	4.91	*3.24	3.05	
Arg26	8.79	4.89	2.12, 1.93		$C^\gamma H$ 1.88, 1.70; $C^\delta H$ 3.37; $N^\epsilon H$ 7.35
Cys27	9.11	5.10	*2.93	3.12	
Ser28	8.92	4.62	4.31, 4.08		
Met29	8.75	4.46	2.23, 2.21		$C^\gamma H$ 2.72
Ile30	7.85	4.40	2.12		$C^{\gamma 2}H$ 0.97; $C^{\gamma 1}H$ 1.44, 1.17; $C^\delta H$ 0.94
Gly31	8.18	4.11, 3.59			
Thr32	7.75	4.70	4.39		$C^\gamma H$ 1.20
Asn33	8.82	4.62	3.12, 2.87		$N^{\delta 2}H$ 7.58, 6.96
Cys34	8.55	5.35	*3.78	2.84	
Glu35	8.95	5.27	*1.89	1.96	$C^\gamma H$ 2.45
Cys36	9.32	5.24	*2.99	2.83	
Thr37	8.57	4.53	4.23		$C^\gamma H$ 1.43
Pro38		4.36	2.26, 1.91		$C^\gamma H$ 2.01, 1.73; $C^\delta H$ 3.44, 3.26
Arg39	8.40	4.33	1.94, 1.90		$C^\gamma H$ 1.75, 1.72; $C^\delta H$ 3.32; $N^\epsilon H$ 7.41
Leu40	8.33	4.42	1.74, 1.67		$C^\gamma H$ 1.66; $C^\delta H$ 1.03, 0.97
Ile41	8.15	4.22	1.96		$C^{\gamma 2}H$ 0.98; $C^{\gamma 1}H$ 1.58, 1.30; $C^\delta H$ 0.94
Met42	8.36	4.53	2.14, 2.08		$C^\gamma H$ 2.67, 2.58
Glu43	8.38	4.44	2.19, 2.05		$C^\gamma H$ 2.54, 2.50
Gly44	8.45	4.08, 4.02			
Leu45	8.12	4.47	1.72, 1.65		$C^\gamma H$ 1.74; $C^\delta H$ 1.02, 0.97
Ser46	8.35	4.43	3.86, 3.81		
Phe47	8.20	4.76	3.30, 3.04		$C^\delta H$ 7.31; $C^\epsilon H$ 7.44; $C^\zeta H$ 7.40
Ala48	8.24	4.35	1.46		

[a] Chemical shifts are reported for the ω-Aga-IVB at pH 4.0 and 300 K in buffer containing 50 mM sodium phosphate and 50 mM sodium acetate. Proton chemical shifts are referenced to H_2O at 4.86 ppm.[b] An asterisk indicates a stereospecific assignment.

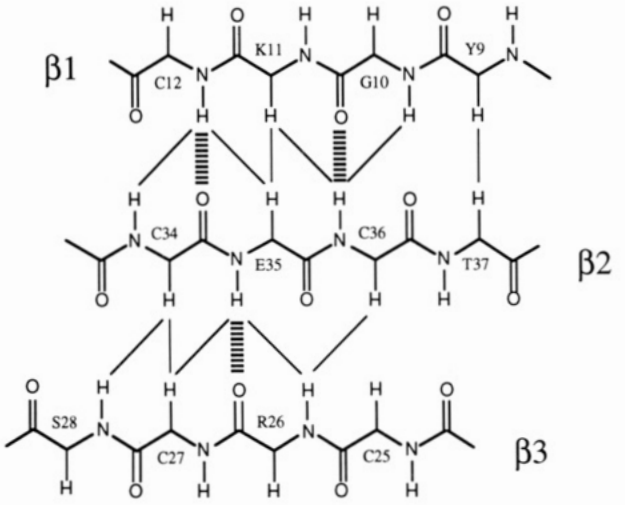

FIGURE 3: Schematic diagram of the interstrand NOEs in the β sheet regions of ω-Aga-IVB. Solid lines indicate interstrand NOEs, and dashed lines show deduced hydrogen bonds from slowly exchanging amide protons and long-range NOEs.

Table II: S–S Distances of the Initial Structures Calculated without the Disulfide Restraints

pattern	disulfide bonds	S–S distances (Å)
I	(12–25)	4.91 ± 0.16
	(19–36)	4.44 ± 0.13
II	(12–36)	6.24 ± 0.12
	(19–25)	7.97 ± 0.26
III	(12–19)	6.64 ± 0.23
	(25–36)	7.33 ± 0.26

N-terminal portion of the protein. The residues of the loop between strand 2 and 3 (from Met29 to Asn33) do not show the NOEs characteristic of a tight reverse turn.

Three-Dimensional Structure Determination. Initial structures of ω-Aga-IVB were based on 455 distance restraints and 27 dihedral restraints (10 ϕ and 17 χ_1). At this stage, no disulfide restraints were used in the calculations. Out of 30 random structures, 26 structures converged with reasonable energies and geometries, which were subsequently refined using a protocol described above. The refined structures showed good agreement with the experimental restraints, having no distance violations greater than 0.3 Å or dihedral angle violations larger than 3°. Excluding the three N-terminal residues (Glu1–Asn3) and the 10 C-terminal residues (Arg39–Ala48) (see below), the average RMSD of the 26 refined structures from the mean coordinates for the backbone atoms is 1.51 ± 0.09 Å. Analysis of the 26 structures showed that two disulfide bonds, Cys4–Cys20 and Cys27–Cys34, could be identified unambiguously. However, the other four cysteines (Cys12, Cys19, Cys25, and Cys36) are clustered together in the core of the protein, leaving three possible disulfide pairing. Table II shows the average value of the six possible intersulfur distances for the four cysteines (Cys12, Cys19, Cys25, and Cys36) measured from the 26 refined structures. On the basis of these distances, pattern I with disulfide pairing of (12–25) and (19–36) is the most reasonable pattern of the three. Although the evidence is significant, it is not definitive. In addition, no $C_\beta H$–$C_\beta H$ NOEs or $C_\alpha H$–$C_\beta H$ NOEs among these cysteines were observed. We therefore generated three sets of structures with the same NOE and dihedral restraints but different disulfide bonding patterns, starting from the 26 refined structures that were generated without disulfide restraints. All three sets of structures have reasonable energies and geometries. However, out of 26 structures calculated with disulfide patterns II and III, 26 and 20 structures, respectively, showed either NOE violations larger than 0.3 Å or dihedral violations greater than 3°. Only 5 out of 26 structures generated with disulfide pattern I contained these violations. Since disulfide pattern I is more consistent with our NMR data, we surmise that the disulfide bonds of ω-Aga-IVB are most likely (4–20), (12–25), (19–36), and (27–34).

Table III: Structural and Energetic Statistics of the Final Set of ω-Aga-IVB Structures

parameter	SA_i	$\langle SA \rangle_{ref}$[a]
RMSDs from Experimental Restraints		
RMS distance deviations (Å)		
all (459)	0.011 ± 0.001	0.006
interproton distances		
intraresidue (183)	0.010 ± 0.001	0.003
interresidue sequential ($\|i-j\| = 1$) (159)	0.013 ± 0.001	0.008
interresidue short-range ($1 < \|i-j\| \leq 5$) (28)	0.004 ± 0.001	0.002
interresidue long-range ($\|i-j\| > 5$) (79)	0.005 ± 0.001	0.004
hydrogen-bond and disulfide bond restraints[b] (10)	0.002 ± 0.001	0.003
RMS dihedral deviations (deg)		
all (27)	0.195 ± 0.041	0.011
Deviations from Idealized Geometry[c]		
bonds (Å) (706)	0.004 ± 0.000	0.004
angles (deg) (1269)	1.202 ± 0.002	1.311
impropers (deg) (288)	0.142 ± 0.006	0.136
Energetic Statistics (kcal mol^{-1})		
E_{repel}[d]	3.6 ± 0.5	1.3
E_{vdW}[e]	–41.7 ± 3.3	–60.5
E_{NOE}[f]	2.7 ± 0.3	0.6

[a] The SA_i column gives the average and standard deviations for the indicated variables obtained from the 21 final refined simulated annealing structures. $\langle SA \rangle_{ref}$ represents the average structure of SA_i least-squares fit to each other including all atoms and refined with 500 steps of steepest-descent energy minimization with the simulated annealing parameters. Distance and angular RMSDs are from the upper or lower bounds of the distance and angular restraints, respectively. [b] The disulfide bond restraints are included as distance restraints only with 1.92 Å $\leq d_{S-S} \leq$ 2.12 Å. [c] Idealized geometries based on CHARMM 19 parameters (Brooks et al., 1983). [d] The value of the quartic repulsive force constant used in the structure calculations was 4 kcal mol^{-1} Å^{-4}. [e] Calculated with standard CHARMM 19 parameters (Brooks et al., 1983). [f] The values of the square-well NOE and torsion angle force constants were 50 kcal mol^{-1} Å^{-2} and 200 kcal mol^{-1} rad^{-2}, respectively.

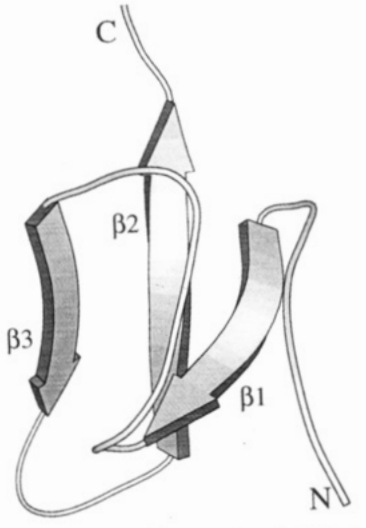

FIGURE 4: Schematic drawing of the tertiary fold of the ω-Aga-IVB. The N- and C-termini are labeled N and C, respectively. The three β strands are labeled β1, β2, and β3. The diagram was generated using the program MOLSCRIPT (Kraulis, 1991).

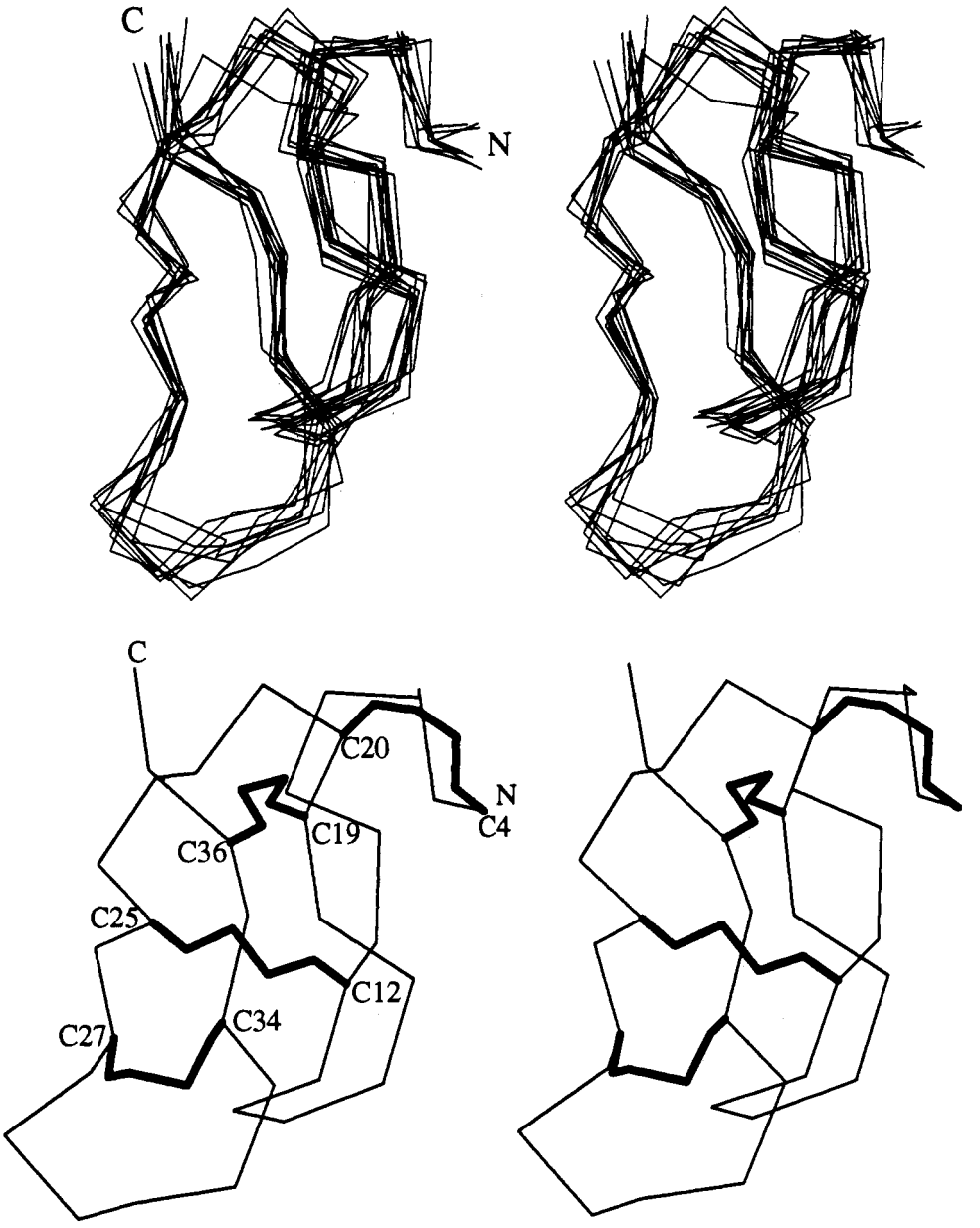

FIGURE 5: (a) Overlay of the 10 C_α traces of the refined ω-Aga-IVB structures that showed lowest RMSD from the average coordinates. The disulfide bonds are not shown for clarity. The N-terminal three residues (Glu1–Asn3) and the C-terminal 10 residues (Arg39–Ala48) are not shown. (b) Stereoview of the C_α trace of the minimized average structure of ω-Aga-IVB. The disulfide bonds are shown in bold.

The energetic and geometric statistics for the 21 final accepted structures with the proposed disulfide bonds are summarized in Table III. Excluding the N-terminal (residues 1–3) and C-terminal (residues 39–48) regions (see below), the average RMSDs for these 21 structures compared to their mean coordinates are 1.17 ± 0.08 Å for the backbone atoms and 1.65 ± 0.08 Å for all heavy atoms. Figure 5 shows a stereoview of the overlay of the 10 best fitted C_α traces.

The hydrophobic core of ω-Aga-IVB is entirely composed of the side chains of cystines Cys12–Cys25 and Cys19–Cys36. Strand β2 and strand β3 are interconnected by disulfide (27–34), while two disulfides (19–36) and (12–25) tie the loop connecting strand β1 and β3 to the β sheet. The disulfide (4–20), together with the hydrophobic residues Ile5 and Tyr9, helps to localize N-terminal region of the protein. Trp14 packs against sulfur atoms from Cys27 and Cys34 and possibly serves to stablize the loop region between β2 and β3.

Although the core of the protein is reasonably well-defined by the NMR data, the N-terminal three residues (Glu1–Asn3) and the C-terminal 10 residues (Arg39–Ala48) are poorly defined. This is supported by two lines of evidence. First, we have not been able to observe any medium-range NOEs within the region or long-range NOEs from the region to the rest of the molecule. Secondly, the amide NH and CαH proton chemical shifts are highly degenerate and cluster near the random-coil values for the individual residues. The flexiblity of the C-terminal tail may have important implications of the toxins biological activity.

DISCUSSION

Biochemical characterization of neuronal voltage-dependent calcium channels has revealed an oligomeric structure comprised of at least three subunits termed α_1, α_2-δ, and β (Catterall, 1991c). The α_1 protein is the central functional component that contains the ion conductance pathway (Ahlijanian et al., 1990). The α_1 subunit believed to be present in the P-type channel has been cloned from rabbit, rat, and human cDNA libraries (Mori et al., 1991; Starr et al., 1991; Barry et al., 1993). On the basis of hydropathy plots and homology to voltage-dependent sodium and potassium chan-

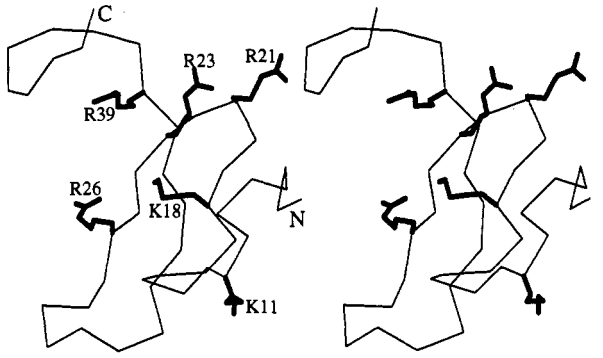

FIGURE 6: Stereoview of the distribution of the positively charged amino acid side chains in ω-Aga-IVB. The side chains of the four arginines and two lysines are shown in bold.

nels, the α_1 subunit of the Ca^{2+} channels is suggested to havefour homologous repeats (I–IV) each with six putative transmembrane helical segments (S1–S6). Segment S4 from each domain is thought to contain the voltage sensor, while S5, S6, and the loop connecting them are intimately involved in the formation of the channel pore (Catterall, 1991b,c; Miller, 1992). A stretch of negatively charged amino acids (9 of 11 residues) is found at the beginning of the extracellular loop between IVS5 and IVS6 of the P-type channel in all three species. This motif is absent from N- and L-type channels and may be important in conferring potency and selectivity to extracellular P-channel antagonists.

The calculated structures are poorly defined through the 10 C-terminal residues (from Arg39 to Ala48). Analysis of the structure also reveals a striking distribution of charged residues. Three of the six positively charged residues (Arg21, Arg23, and Arg39) are found in close proximity to the point at which the flexible hydrophobic tail attaches to the body of the protein (Figure 6) and are conserved in the related toxin ω-Aga-IVA. Combined with the suggestion that there are clusters of negatively charged residues near the pore of the channel, one speculative model of the interaction of the toxin and the channel has emerged. The complementary electrostatic attractions between the toxin and the extracellular loops near the mouth of the pore may contribute to binding affinity, while the toxin's hydrophobic tail may cause the blockade of the channel either simply by occluding the conductance pathway or by establishing additional molecular contacts with the channel protein. An alternative mechanism would view the C-ternimal tail as a nonspecific hydrophobic anchor and would deposit the toxin in the lipid bilayer. Interaction between the toxin and the channel would commense at the lipid/channel protein interface. These proposed mechanisms suggest additional experiments that could assess the biological importance of the C-terminal tail. With regard to the first model, a C-terminally truncated toxin would not be expected to inhibit the current carried by P-channels. Yet such a tailless toxin might be expected to abrogate the antagonism of full length ω-Aga-IVA or B. In considering the second model, a panel of toxins sequentially truncated or elongated by one amino acid would show a gradual decrease or increase in potency, respectively. Moreover, the tail could be replaced either by a sequence of similar hydrophobicity or a surrogate membrane anchor and retain biological activity. It is interesting to note that a calcium channel toxin isolated from *Plectreurys trites*, PLTX-II, maintains a cysteine-rich protein core and has a C-terminal palmitoyl group that is necessary for its biological activity (Branton et al., 1992). Experiments designed to test these predictions are now in progress.

ADDED IN PROOF

After submission of this paper, a partial disulfide map for ω-Aga-IVB was determined using enzymatic cleavage analysis. The analysis established the presence of the Cys12–Cys25 disulfide bond and indicated that Cys19 and Cys20 are not disulfide-bonded to each other. The partial mapping is consistent with the data reported herein.

ACKNOWLEDGMENT

We thank Bruker Instruments for providing instrument time and Dr. C. Anklin and Dr. W. Massefski for assistance with the acquisition of the NMR data. We thank WPS Pharmaceuticals for generous venom supply. M.K.R. is a recipient of a fellowship from the American Chemical Society and Merck Sharp & Dohme Research Laboratories.

REFERENCES

Ahlijanian, M. K., Westenbroek, R. E., & Catterall, W. A. (1990) *Neuron 4*, 819–832.
Augustine, G. J., Charlton, M. P., & Smith, S. J. (1987) *Annu. Rev. Neurosci. 10*, 633–693.
Barry, E. L. R., Viglione, M. P., OShaughnessy, T. J., Froehner, S. C., & Kim, Y. I. (1993) *Biophys. J. 64*, A318.
Bax, A., & Davis, D. (1985) *J. Magn. Reson. 65*, 355–360.
Bax, A., Freeman, R., Frenkiel, T. A., & Levitt, M. H. (1981) *J. Magn. Reson. 43*, 478–483.
Bean, B. P. (1989) *Annu. Rev. Physiol. 51*, 367–384.
Branton, W. D., Rudnick, M. S., & Zhou, Y. (1992) *Soc. Neurosci. Abstr. 18*, 10.
Brooks, B. R., Bruccoleri, R. E., Olafson, B. D., States, D. J., Swaminathan, S., & Karplus, M. (1983) *J. Comput. Chem. 4*, 187–217.
Brünger, A. T. (1990) *X-PLOR Manual (Version 2.1)*, Yale University, New Haven, CT.
Brünger, A. T. (1993) *X-PLOR Manual (Version 3.1)*, Yale University, New Haven, CT.
Burke, S. P., Taylor, C. P., & Adams, M. E. (1992) *Soc. Neurosci. Abstr. 18*, 9.
Castle, N. A., Haylett, D. G., & Jenkinson, D. H. (1989) *Trends Neurosci. 12*, 59–65.
Catterall, W. A. (1984) *Science 223*, 653–661.
Catterall, W. A. (1991a) *Cell 64*, 871–874.
Catterall, W. A. (1991b) *Curr. Opin. Neurobiol. 1*, 5–13.
Catterall, W. A. (1991c) *Science 253*, 1499–1500.
Chazin, W. J., & Wright, P. E. (1988b) *J. Mol. Biol. 202*, 623–636.
Chazin, W. J., Rance, M., & Wright, P. E. (1988a) *J. Mol. Biol. 202*, 603–622.
Dubel, S. J., Starr, T. V. B., Hell, J., Ahlijanian, M. K., Enyeart, J. J., Catterall, W. A., & Snutch, T. P. (1992) *Proc. Natl. Acad. Sci. U.S.A. 89*, 5058–5062.
Eich, G., Bodenhausen, G., & Ernst, R. R. (1982) *J. Am. Chem. Soc. 104*, 3731–3732.
Ganong, A. H., et al. (1993) *Soc. Neurosci. Abstr.* (submitted).
Hare, D. (1991) *FELIX manual (Version 2.0)*, Hare Research, Inc.
Hess, P. (1990) *Annu. Rev. Neurosci. 13*, 1337–1356.
Hirning, L. D., Artman, L. D., Alasti, N., Phillips, D., Volkmann, R. A., Saccomano, N. A., & Mueller, A. L. (1992) *Soc. Neurosci. Abstr. 18*, 970.
Hirning, L. D., Alasti, N., Phillips, D., Lanzetti, A. M., Volkmann, R. A., Saccomano, N. A., Mueller, A. L., & Artman, L. D. (1993) *J. Biol. Chem.* (submitted).
Jeener, J., Meier, B. H., Bachmann, P., & Ernst, R. R. (1979) *J. Chem. Phys. 71*, 4546–4553.
Kabsch, W., & Sander, C. (1983) *Biopolymers 22*, 2577.
Kater, S. B., Mattson, M. P., Cohan, C., & Connor, J. (1988) *Trends Neurosci. 11*, 315–321.
Kennedy, M. B. (1989) *Trends Neurosci. 12*, 417–420.
Kraulis, P. J. (1991) *J. Appl. Crystallogr. 24*, 946–950.

Llinas, R. R. (1988) *Science 242*, 1654–1664.
Llinas, R. R., Sugimori, M., Lin, J. W., & Cherksey, B. (1989) *Proc. Natl. Acad. Sci. U.S.A. 86*, 1689–1693.
Llinas, R. R., Sugimori, M., Hillman, D. E., & Cherksey, B. (1992) *Trends Neurosci. 15*, 351–355.
Macura, S., Huang, Y., Suter, D., & Ernst, R. R. (1981) *J. Magn. Reson. 43*, 259–281.
Miller, C. (1992) *Curr. Biol. 2*, 573–576.
Mintz, I. M., Venema, V. J., Swiderek, K. M., Lee, T. D., Bean, B. P., & Adams, M. E. (1992) *Nature 355*, 827–829.
Mori, Y., et al. (1991) *Nature 350*, 398–402.
Murphy, T. H., Worley, P. F., & Baraban, J. M. (1991) *Neuron 7*, 625–635.
Olivera, B. M., MaacIntosh, J. M., Cruz, L. J., Luque, F. A., & Gray, W. R. (1984) *Biochemistry 23*, 5087–5090.
Phillips, D., Saccomano, N. A., & Volkmann, R. A. (1992) U.S. Patent No. 5,122,596, filed September 29, 1989.
Piantini, U., Sørensen, W., & Ernst, R. R. (1982) *J. Am. Chem. Soc. 104*, 6800–6801.
Regan, L. J. (1991a) *J. Neurosci.* 11, 2259–2260.
Regan, L. J., Sah, D. W. Y., & Bean, B. P. (1991b) *Neuron 6*, 269–280.
Spedding, M., & Paoletti, R. (1992) *Pharmacol. Rev. 44*, 363–376.
Starr, T. V. B., Prystay, W., & Snutch, T. P. (1991) *Proc. Natl. Acad. Sci. U.S.A. 88*, 5621–5625.
Tsien, R. W., Lipscombe, D., Madison, D. V., Bley, K. R., & Fox, A. P. (1988) *Trends Neurosci. 11*, 431–438.
Tsien, R. W., Ellinor, P. T., & Horne, W. A. (1991) *Trends Pharmacol. Sci. 12*, 349–354.
Turner, T. J., Adams, M. E., & Dunlap K. (1992) *Science 258*, 310–313.
Wagner, G., Braun, W., Havel, T. F., Schaumann, T., Go, N., & Wüthrich, K. (1987) *J. Mol. Biol. 196*, 611–639.
Weiss, J. H., Hartley, D. M., Koh, D. M., & Choi, D. W. (1990) *Science 247*, 1474–1477.
Williams, M. E., et al. (1992) *Science 257*, 389–395.
Williams, R. J. P. (1989) *Eur. J. Biochem. 183*, 479–497.
Wishart, D. S., Sykes, B. D., & Richards, F. M. (1992) *Biochemistry 31*, 1647–1651.
Wüthrich, K. (1986) *NMR of Proteins and Nucleic Acids*, Wiley, New York.